Higher temperature enhances spatio-temporal concentration of rainfall

Kaihao Long[1], Dagang Wang[1], Guiling Wang[2], Jinxin Zhu[1], Shuo Wang[3], Shuishi Xie[4]

[1]School of Geography and Planning, Sun Yat-Sen University, Guangzhou, Guangdong Province, China

[2]Department of Civil and Environmental Engineering, University of Connecticut, Storrs, Connecticut, USA

[3]Department of Land Surveying and Geo-Informatics, The Hong Kong Polytechnic University, Hong Kong, China

[4]Ganzhou Hydrological Bureau, Ganzhou, Jiangxi Province, China

Submitted to Journal of Hydrometeorology

February 24th, 2021, submitted

October 3rd, 2021, revised Corresponding author: Dagang Wang,

wangdag@mail.sysu.edu.cn

Abstract

The relationship between extreme precipitation intensity and temperature has been comprehensively studied over different regions worldwide. However, the effect of temperature on the spatio-temporal organization of precipitation, which can have a significant impact on precipitation intensity, has not been adequately studied or understood. In this study, we propose a novel approach to quantifying the spatial and temporal concentration of precipitation at the event level and study how the concentration varies with temperature. The results based on rain gauge data from 843 stations in the Ganzhou county, a humid region in south China, show that rain events tend to be more concentrated both temporally and spatially at higher temperature, and this increase in concentration qualitatively holds for events of different precipitation amounts and durations. The effects of temperature on precipitation organization in space and in time differ at high temperatures. The temporal concentration increases with temperature up to a threshold (approximately 24°C) beyond which it plateaus, whereas the spatial concentration keeps rising with temperature. More concentrated precipitation, in addition to a projected increase of extreme precipitation, would intensify flooding in a warming world, causing more detrimental effects.

Keywords: spatio-temporal organization of precipitation; rainfall concentration index; temperature; rain event

1. Introduction

Global climate changes have been observed with an evident increase in both temperature and precipitation throughout the last century (Alexander et al. 2006). An important consequence of a warming climate is the increase of precipitation extremes, as supported by both observational and model-based studies (Christensen and Christensen 2004; Wang et al. 2007; Papalexiou and Montanari 2019). As intensified extreme precipitation events likely cause more serious damage to the ecosystems, economy, and society (Chen et al. 2012; Pei et al. 2016; Peleg et al. 2020; Weyhenmeyer et al. 2004), assessing the impact of temperature on precipitation and possible future changes of precipitation events is crucial for guiding climate adaptation efforts.

Previous studies on the relationship between precipitation and temperature focus mostly on how precipitation amount and intensity change with rising temperature and what factors confound this relationship. According to the Clausius-Clapeyron (CC) equation, the capacity of the atmosphere to hold water vapor increases with rising temperature at a rate of about 7% per °C (termed as the CC scaling rate), thus extreme precipitation intensity is expected to increase with temperature at a similar rate (termed as the precipitation scaling). However, observations demonstrate that the local precipitation scaling is not always consistent with the CC scaling rate. A quasi-global assessment of the precipitation-temperature relation (Wasko et al. 2016a) shows that precipitation scaling greatly varies with region, ranging from negative scaling to double CC scaling. Further studies imply that the precipitation scaling may be influenced by relative humidity (Hardwick Jones et al. 2010), time scale (Utsumi et al. 2011), and even precipitation type (Berg et al. 2013). Recent studies show that the scaling can be quite consistent if proper methods are used. For example, Visser et al. (2020) found that the extreme precipitation-temperature scaling is quite consistent across Australia when using the dry-bulb temperature just prior to precipitation. The use of dew-point temperature also helps increase the consistency in such scaling (Fowler et al. 2021). However, the rate of precipitation scaling with temperature still varies across regions. In a recent study, Lochbihler et al. (2017) pointed out that the higher rate of precipitation scaling tends to coincide with a larger spatial extent, which highlights the importance of the spatial rainfall characteristics in explaining the precipitation-temperature relationship. Furthermore, how the spatio-temporal characteristics of precipitation might change with temperature bears direct relevance to the scaling of precipitation intensity.

How temperature influences the spatio-temporal characteristics of precipitation has been tackled by several recent studies. Wasko and Sharma (2015) found that the temporal distribution of rainfall tends to be less uniform in warmer environments based on measurements at 79 gauge stations in Australia. Using the same measurements in Australia, Wasko et al. (2016b) show that rainfall is more concentrated in the storm center with a reduced spatial extent at high temperature, which was subsequently confirmed by a modeling study on the Greater Sydney region (Li et al. (2018)). Based on high-resolution weather radar data over the Mediterranean, Peleg et al. (2018) found the storm area decreases with warmer temperatures. Consistent with the observational evidence, climate models also projected substantially higher intensity of heavy precipitation in a warmer climate under the future emission scenarios (Prein et al., 2017; Rastogi et al. 2020). These studies were carried out for relatively dry climate zones in Australia and the Mediterranean, and focused on the impact of temperature on either temporal or spatial organization. A more comprehensive study is needed to investigate the precipitation organization in both space and time and its relationship with temperature, especially for relatively humid climate regimes.

The temporal or spatial concentration of precipitation, which is an indicator of rainfall distribution over time or space, is an important feature of rainfall events. Different indices have been proposed to quantify precipitation concentration. For temporal concentration, Martin-Vide (2004) proposed the Concentration Index (CI), which measures the ratio of heavy rain to total rainfall, based on the Gini index concept to quantify the unevenness of long precipitation time series. Although CI is widely used to characterize the temporal concentration of daily rainfall, it requires data with a long time series and thus not suitable for rainfall analysis at the event scale. Another index termed Precipitation Concentration Index (PCI) measures the temporal unevenness of precipitation, based on the deviation between the square of sum and the quadratic sum of precipitation series (Oliver 2010). PCI has been used to evaluate the concentration of precipitation series at different time scales, such as the monthly scale (de Luis et al. 2011) and the seasonal scale (de Luis et al. 2010). The advantage of PCI is that it can be applied to precipitation time series of any length. However, the PCI-based results are not comparable between precipitation time series of different lengths, as the length of data has a direct influence on the results. As for spatial concentration, Lochbihler et al. (2017)

defined the spatial extent of rainfall as the square root of the continuous area with rainfall intensity exceeding a threshold and applied this definition to the evaluation of spatial precipitation concentration. Wasko et al. (2016b) used the concept of effective radius, which is a precipitation-weighted distance from the centroid of the storm, to assess how spatially concentrated the storm is.

Existing indices pertain to rainfall concentration either in space or in time. A unified approach applicable to concentration in both space and time is lacking. Moreover, existing indices cannot reflect the nature of the spatio-temporal organization in a way relevant to flood risk. In addition, it is not clear whether the rainfall concentration-temperature relationship found in arid and Mediterranean climates might hold in more humid climate regimes. In this paper, we propose new indices to represent temporal and spatial concentration at the rain event scale in a unified framework; we then apply the definitions and their calculations to precipitation gauge measurements and investigate how the precipitation concentration might change with temperature.

2. Study Area, Data, and Methods

In this paper, we take Ganzhou, a county located in Jiangxi province, China, as our study area. Ganzhou is 39380 km^2 in area, covering longitude 113.5°E – 117.0°E and latitude 24.5°N – 27.5°N with a subtropical humid monsoon climate. Two types of data, rainfall, and temperature are used for analysis. The rainfall dataset is from measurements at gauge stations in the Ganzhou region, which contains 843 valid rainfall stations and spans a period of 5 years from 2013 to 2018 (Figure 1). The gauge stations are quite evenly distributed over the region. Snowfall is excluded from the analysis as it rarely occurs in this region and cannot be accurately measured by the tipping bucket at the gauge stations. Rainfall data is recorded at a 5-minute interval for each rain event. As for temperature data, due to the absence of temperature records from the rain gauge stations, we use a gridded temperature data, the CMA Land Data Assimilation System (CLDAS) 2-meter air temperature (Zhao et al. 2018) as surrogates for gauge measurements in this study. The CLDAS temperature dataset has a temporal resolution of 1 hour and a spatial resolution of 0.0625°. As spatial scales are different between rain gauge measurements and CLDAS temperature, we match the rainfall data at each station with the temperature data at the CLDAS grid cell encompassing the gauge station.

With the paired rainfall and temperature data, we split the time series data into a number of rain events according to the duration between two events, and this is done for each station separately. To define rain events, we take a threshold that is five times of the data temporal resolution following the approach of Wasko et al. (2016b). Specifically, if the dry period between two continuous series of rain is longer than five times of the temporal resolution (i.e., 25 minutes), these two series are considered as two separate rain events. We finally obtain 242841 rain events from the original data. Figure 2 shows the statistics of these rain events, including the number of rain events and their spatial distribution, and histograms of rain duration and amount. The number of events at each station approximately ranges from 150 to 400. Most events last less than 14 hours, with rain amount less than 100 mm.

We calculate the rainfall amount, duration, and the concurrent temperature for each rain event, where the concurrent temperature is estimated as the arithmetic mean of hourly temperature during the rain event.

Inspired by the concept of CI proposed by Martin-Vide (2004), we propose new indices to represent the concentration of rainfall in time and space, respectively for rainfall events within a unified framework. Conceptually, the temporal concentration index (TCI) of a rain event measures the deviation of the cumulative rainfall over any portion of an actual rain event from that of an assumed evenly distributed rain event with the same amount. For each event, the cumulative series include cumulative rain amounts corresponding to durations surrounding the temporal center of the event (i.e., the most concentrated point in the temporal distribution of rainfall). For any given temporal center, the accumulation starts with rainfall in the interval at the temporal center; rainfall is then added to the accumulation one interval at a time, starting from the interval(s) closest to the temporal center and extending outward. For intervals with the same time difference from the temporal center, the interval with more rainfall is added first. It is important to identify the temporal center of rain events in calculating TCI. However, automatically identifying the center is challenging, as the time point at which the strongest rain occurs is not always the temporal center in a rain event. For practical use, we calculate TCI using each time point during a rain event as the hypothetical temporal center; the largest TCI identifies the true temporal center and is taken as the final TCI of the event. As shown in Figure 3, the detailed calculation procedure has 5 steps:

Step 1. choose a time point as the hypothetical temporal center, and mark this point as time ID 1 (Figure 3a).

Step 2. mark the two time points next to the temporal center as time IDs 2 and 3 (the point with larger rainfall in these two points ranks higher), and mark the remaining time points as time IDs 4, 5, and so on (Figure 3a).

Step 3. calculate the cumulative rainfall corresponding to each ID, and plot the curve for the cumulative rainfall vs. accumulation time. The curve starts from the coordinate origin (0, 0) and ends at (T, P) where T and P are the duration and total rainfall of the rain event, respectively (Figure 3a).

Step 4. calculate the difference between the curve of actual rain event obtained in step 3 (Figure 3b) and the straight line that represents an evenly distributed rain event (Figure 3c). The difference is represented by the area dA enclosed by the curve and the straight line connecting (0, 0) and (T, P) in Figure 3d. The ratio of dA to the triangle area A is the TCI for the chosen temporal center in a rain event, i.e., to what degree rainfall is concentrated around the chosen time point during the event. It is noted that the areas above the straight line are taken with a positive sign, whereas those under the straight line are taken with a negative sign.

Step 5. treat each remaining time points as the hypothetical temporal center and repeat steps 1-4 to calculate TCI (Figure 3e).

At the end of step 5, every time point during the rain event will have a corresponding TCI value; the time point with the largest TCI value is the actual temporal center of the rain event, and the corresponding TCI value is considered the final TCI of the rain event (Figure 3e).

The final TCI varies from 0 to 1. More exactly, it is equal to or greater than 0, and less than 1, as rainfall is not possibly concentrated in a nearly zero interval. An index value closer to 1 indicates that rainfall is highly concentrated in time, whereas the value closer to 0 means a more uniform rain event. This is not without exception. For an idealized, temporally symmetric bi-modal rainfall process that reaches its maximum intensity at the very beginning and very end of the event, the event TCI value approaches or may even equals zero. However, this type of events is extremely rare in reality and is non-existent in our station records; most events start and/or end with lighter rain, which effectively steers the TCI value away from zero towards a positive value. This exception therefore does not affect the results and the conclusion of this study. The range between 0 and 1 makes TCI comparable among rain events of different durations. In addition, TCI represents the temporal concentration around the temporal center in a rain event instead of the unevenness of a rain series. This is of great significance for flooding, as more concentrated rainfall around the rain center with a large amount of total rainfall can lead to a more disastrous flood.

Similar to the concept of TCI, we propose a spatial concentration index (SCI) to represent how rainfall concentrates in space for a rain event. First, we define the rain event from the spatial perspective following Wasko et al. (2016b). A spatial event for any central gauge is defined by concurrent rainfall at neighboring gauges within a radius of 20 km from the central gauge in a 5-minute temporal interval, and SCI is calculated for each spatial event. As such, a rain event is recorded as a set of stations and their corresponding rainfall amounts from the spatial perspective (Figure 4a). We then plot the rain amount at each station (including the central station and its neighboring stations) according to its distance from the central station, as shown in Figure 4b. Similar to the procedure in calculating TCI, we take the central station as the assumed spatial center, calculate the accumulative rainfall with respect to distance (red line in Figure 4c), and estimate the relative difference in the cumulative rainfall between the actual rain event and an assumed evenly distributed rain event with the same total amount. A meaningful SCI value for a spatial rain event largely relies on the selection of the spatial center of the event. To identify the spatial center, we use a similar method used to identify the temporal center in the TCI calculation. We take each station as the presumable spatial center and calculate the corresponding SCI using the aforementioned procedure, and adopt the largest SCI as the final SCI for a specific rain event. The range of the final SCI is between 0-1, similar to TCI.

With the proposed TCI and SCI, we calculate the values of the two indices for all rain events, and study the characteristics of the indices and their relationships with temperature. It is noted that temperature for a rain event in the TCI calculation is estimated as the arithmetic mean of hourly temperature during the event, and the estimates of temperature for a spatial rain event in the SCI calculation is based on the arithmetic mean of temperature on the grid cells within the radius threshold.

3. Results and Discussions

a. Temporal concentration of rain events and its relation with temperature

To minimize the uncertainty associated with short-duration events, we remove all events shorter than 1 hour, and only keep those that are more than 1 hour in duration (i.e., with 12 or more time steps) for the analysis. Figure 5a shows the distribution of TCI values of all the selected events. The distribution of TCI can be well described by a Beta distribution function, indicating that rain events with different temporal concentrations do not occur with the same probability. Events with moderate temporal concentration (around 0.2 of TCI) occur more frequently, whereas those with high temporal concentration and those with nearly uniform distribution account for a small portion of total events.

Furthermore, to explore the effect of temperature on the distribution of temporal concentration of rain events, we divide the events into two groups according to temperature: one containing events occurring at temperatures lower than 20°C, and the other containing the rest. Figure 5b shows the corresponding TCI distribution for the two groups of rain events, which can also be described by a Beta distribution. Both the sample distribution and the fitted Beta distribution of TCI (Figure 5b) indicates that the two temperature groups differ from each other. A Kolmogorov–Smirnov (K-S) test applied to the cumulative distributions indicates the difference is statistically significant, which is verified by a close-to-zero p-value (Figure 5c) and sufficiently large sample sizes of the two groups (Figure 5d). Most events in the lower temperature group have TCI values ranging from 0.2 to 0.4 and fewer events have TCI values greater than 0.4, whereas approximately half of the events in the higher temperature group have TCI values greater than 0.4. This indicates a potential dependence of the temporal concentration of rain events on temperature, i.e., rain events may be more temporally concentrated under warmer conditions.

To confirm this assumption, we carry out further analysis using a binning method. With a compromise between the number of bins and the sample size in each bin, we choose a bin size of 2 °C and divide the events with temperature ranging from 5 to 30 °C into 12 bins, and calculate the average TCI values within each bin. It is evident that the bin-average TCI value increases with temperature within the range of 5 to 24 °C and plateaus at temperatures beyond 24°C (Figure 6a). Similar results are obtained when stratifying the analysis according to event-scale rainfall amount (e.g., 50th, 75th, and 90th percentiles). The increasing trends of all groups in Figure 6a are significant at the 99% confidence level, which is supported by the statistical test with a Spearman correlation method. The 95% confidence interval of the TCI-temperature curve for all events is small (Figure 6b). The ascending pattern of the temporal concentration with increasing temperature within the range of 5 to 24 °C is consistent with the findings of Wasko and Sharma (2015) that higher temperatures induce a less uniform temporal pattern (i.e., a temporally more concentrated pattern) of rainfall. Besides, our results seem to reveal a temperature threshold beyond which the increase of the bin-average TCI stagnates. The threshold of 24 °C is similar to the peak-point temperature in the precipitation scaling with temperature (Utsumi et al. 2011; Xiao et al. 2016).

The peak structure of the relationship between extreme precipitation intensity and temperature is widely observed over the globe (Wang et al. 2017). Extreme precipitation increases with temperature below a temperature threshold beyond which extreme precipitation plateaus or even decreases with the increase of temperature. There are several possible underlying mechanisms for the peak structure. For instance, Utsumi et al. (2011) found that the decrease of the rain duration could well explain why extreme daily precipitation intensity decrease at higher temperatures. Hardwick Jones et al. (2010) suggested that moisture availability is the dominant driver of how extreme precipitation scales with rising temperature. A similar temperature threshold for the relationship between temporal precipitation concentration and temperature found in our study may offer a new clue to explain the behavior of extreme precipitation at high temperature. That is, the limited temporal concentration of precipitation events at higher temperatures may be one of the reasons why extreme precipitation intensity does not continue to increase at higher temperature, a topic warranting further studies in the future.

We investigate the effect of rain duration on the temporal concentration-temperature relationship by dividing the events into four groups according to the rain duration (Figure 6c). The events with durations of 1-2 hours, 2-3 hours, and 3-4 hours account for 33.8%, 23.7%, and 15.5% of total rain events, respectively. Similarly, the TCI increases with rising temperature within the range of 5 to 24 ℃ and plateaus at temperatures higher than 24 ℃. However, rain events with shorter durations tend to have higher temporal concentration under the same temperature range, as convective rain accounts for the majority of short-duration rain events and is usually more concentrated. In general, Figure 6 confirms the robustness of the relationship between the rainfall temporal concentration and temperature, no matter how long a rain event lasts. However, different temperature sampling (e.g. use of pre-storm temperature or dew point) may influence the results (Visser et al., 2020), and such potential sensitivity will be explored in followup research.

Event separation is the first step in the aforementioned analysis and is accomplished by comparing the dry period between any two rainfall series against a threshold. To examine the results sensitivity to this duration threshold, we experiment on separating rain events using different thresholds (e.g., 50 and 75 minutes) besides the 25 minutes used in the primary analysis. The TCI characteristics and their relationship with temperature remain similar when a different separation threshold is used (Figure 7), suggesting that the TCI-temperature relationship is independent of how rain events are separated.

b. Spatial concentration of rain events and its relation to temperature

Using a similar approach, we study the relationship between the spatial concentration of rain events and temperature. Figure 8 shows the SCI distribution and how it differs between warmer (above 20℃) and cooler (below 20℃) conditions. Different from the Beta distribution for TCI (Figure 5), SCI is better described by a Wald distribution (Figure 8a). Similar to TCI, the SCI distribution is significantly different between the two temperature groups based on a K-S test (Figure 8b-8d). The bin-average SCI continually increases with temperature in the full temperature range when all events are lumped together, and its 95% confidence interval is quite small (Figure 9a and 9b). A similar SCI-temperature relationship is found when the analysis is stratified according to rain amount, showing little difference between low- and high-percentile events (Figure 9a). The increase of SCI with temperature is consistent with the finding of Wasko et al. (2016b) that storms become spatially more concentrated at higher temperatures with an increase of the peak precipitation intensity and a decrease of the spatial extent. Comparing Figure 6a with Figure 9a, we can find that the spatial concentration index keeps rising as temperature increases, which is different from the relationship between the temporal concentration and temperature. This may reveal that the underlying mechanisms are different between the spatial dimension and the temporal dimension in terms of how temperature affects the concentration. Water vapor redistribution in space under warmer conditions is considered as the main reason for higher concentration with rising temperature (Wasko et al. 2016b). Moreover, our results also indicate that rain events with longer durations tend to be more evenly distributed in space (Figure 9c), which is similar to the effect of duration on the temporal concentration (Figure 6c). Note that the study area is located in south China with a subtropical climate. Both frontal and convective rain are common. The majority of the long-duration rain events are of frontal type, which usually spread relatively uniformly over a large region. The scaling rate of TCI and SCI with temperature indicated by Figure 6a and Figure 9a do not show clear spatial variation (not shown), probably because the study region is not large enough and does not span different climate regimes.

The radius used to identify neighboring gauges for any given central gauge is a key parameter in defining the spatial event, and its value may influence the SCI characteristics and their relationship with temperature. To examine its impact on the results, we carry out a sensitivity experiment in which the same SCI analysis procedure is repeated multiple times, each with a different radius. As shown in Figure 10, the SCI-temperature relationships are very similar under different radiuses, which confirms the robustness of the relationship.

4. Summary

In this study, we propose a novel approach to quantifying the precipitation concentration in both time and space at the rain event level and study how the concentration changes with temperature. The proposed approach defines the temporal concentration and the spatial concentration of precipitation in a unified framework. Different from previous indices that characterize the unevenness of precipitation time series, the concentration indices defined in this study reflect how rainfall is concentrated around the temporal or spatial center, which is a more relevant indicator for flood risks.

Results based on analysis of rain gage data from 843 stations in a humid region of China show that rainfall events tend to be more concentrated both temporally and spatially under higher temperature. This suggests that warmer condition not only increases the moisture holding capacity of the atmosphere thus increasing rain intensity, but also enhances the spatio-temporal concentration of rain events. The temperature-induced concentration enhancement in both space and time are robust, and do not depend on rain amount and duration. The spatial concentration of rainfall continues to increase with rising temperature, whereas the temporal concentration plateaus when temperature exceeds a certain threshold. However, this should be interpreted with caution, as the number of bins with temperature higher than 24℃ is limited, and the sample size within each bin is small too.

More concentrated precipitation, in addition to a projected increase of extreme precipitation, would intensify flooding in a warmer world, causing more detrimental effects. The spatial and temporal concentration indices proposed in this study therefore provide important new metrics of precipitation characteristics that are highly relevant for evaluating flood risks in a changing climate. As the relationship between precipitation concentration and temperature may depends on the background climate, follow−up research should explore this topic across different climate regimes to test whether findings from this study may be transferable to other regions.

Acknowledgments

This study was supported by the National Natural Science Foundation of China (Grant No. 51779278, 52079151 to Dagang Wang) and the National Science Foundation (AGS-1659953 to Guiling Wang).

Data Availability Statements

The CLDAS temperature data is downloadable at its official website (http://tipex.data.cma.cn/) after registration and login. The station precipitation data are owned by Ganzhou Hydrological Bureau, and is not freely accessible in the public domain. The station data is accessible by sending an email to the corresponding author (wangdaga@mail.sysu.edu.cn) with a reasonable request.

References

Alexander, L. V., and Coauthors, 2006: Global observed changes in daily climate extremes of temperature and precipitation. *Journal of Geophysical Research*, **111**.

Berg, P., C. Moseley, and J. O. Haerter, 2013: Strong increase in convective precipitation in response to higher temperatures. *Nat Geosci*, **6,** 181-185.

Chen, M. J., C. Y. Lin, Y. T. Wu, P. C. Wu, S. C. Lung, and H. J. Su, 2012: Effects of extreme precipitation to the distribution of infectious diseases in Taiwan, 1994-2008. *Plos One*, **7,** e34651.

Christensen, O. B., and J. H. Christensen, 2004: Intensification of extreme European summer precipitation in a warmer climate. *Global Planet Change*, **44,** 107-117.

de Luis, M., J. C. González-Hidalgo, M. Brunetti, and L. A. Longares, 2011: Precipitation concentration changes in Spain 1946–2005. *Natural Hazards and Earth System Sciences*, **11,** 1259-1265.

de Luis, M., M. Brunetti, J. C. Gonzalez-Hidalgo, L. A. Longares, and J. Martin-Vide, 2010: Changes in seasonal precipitation in the Iberian Peninsula during 1946–2005. *Global and Planetary Change*, **74,** 27-33.

Fowler, H. J., and Coauthors, 2021: Anthropogenic intensification of short-duration rainfall extremes. *Nature Reviews Earth & Environment*, **2,** 107-122.

Hardwick Jones, R., S. Westra, and A. Sharma, 2010: Observed relationships between extreme sub-daily precipitation, surface temperature, and relative humidity. *Geophysical Research Letters*, **37**.

Li, J., C. Wasko, F. Johnson, J. P. Evans, and A. Sharma, 2018: Can Regional Climate Modeling Capture the Observed Changes in Spatial Organization of Extreme Storms at Higher Temperatures? *Geophysical Research Letters*, **45,** 4475-4484.

Lochbihler, K., G. Lenderink, and A. P. Siebesma, 2017: The spatial extent of rainfall events and its relation to precipitation scaling. *Geophysical Research Letters*, **44,** 8629-8636.

Martin-Vide, J., 2004: Spatial distribution of a daily precipitation concentration index in peninsular Spain. *Int J Climatol*, **24,** 959-971.

Oliver, J. E., 2010: Monthly Precipitation Distribution: A Comparative Index. *The Professional Geographer*, **32,** 300-309.

Papalexiou, S. M., and Montanari, A., 2019 : Global and regional increase of precipitation extremes under global warming. *Water Resources Research*, 55, 4901–4914.

Pei, Q., D. D. Zhang, G. D. Li, P. Foret, and H. F. Lee, 2016: Temperature and precipitation effects on agrarian economy in late imperial China. *Environmental Research Letters*, **11**.

Peleg, N., C. Skinner, S. Fatichi, and P. Molnar, 2020: Temperature effects on the spatial structure of heavy rainfall modify catchment hydro-morphological response. *Earth Surface Dynamics*, **8,** 17-36.

Peleg, N., P. Burlando, A. Sharma, E. Morin, P. Molnar, S. Fatichi, and F. Marra, 2018: Intensification of Convective Rain Cells at Warmer Temperatures Observed from High-Resolution Weather Radar Data. *Journal of Hydrometeorology*, **19,** 715-726.

Prein, A.F., Liu, C., Ikeda, K., Trier, S.B., Rasmussen, R.M., Holland, G.J., Clark, M.P., 2017. Increased rainfall volume from future convective storms in the US. Nature Climate Chang. 7, 880-884.

Rastogi, D., D. Touma, K. J. Evans, and M. Ashfaq, 2020: Shift Toward Intense and Widespread Precipitation Events Over the United States by Mid-21st Century. *Geophysical Research Letters*, **47**.

Utsumi, N., S. Seto, S. Kanae, E. E. Maeda, and T. Oki, 2011: Does higher surface temperature intensify extreme precipitation? *Geophysical Research Letters*, **38**.

Visser, J. B., C. Wasko, A. Sharma, and R. Nathan, 2020: Resolving Inconsistencies in Extreme Precipitation-Temperature Sensitivities. *Geophysical Research Letters*, **47**.

Wang, G., D. Wang, K. E. Trenberth, A. Erfanian, M. Yu, Michael G. Bosilovich, and D. T. Parr, 2017: The peak structure and future changes of the relationships between extreme precipitation and temperature. *Nat Clim Change*, **7,** 268-274.

Wasko, C., and A. Sharma, 2015: Steeper temporal distribution of rain intensity at higher temperatures within Australian storms. *Nat Geosci*, **8,** 527-529.

Wasko, C., R. M. Parinussa, and A. Sharma, 2016a: A quasi-global assessment of changes in remotely sensed rainfall extremes with temperature. *Geophysical Research Letters*, **43,** 12,659-612,668.

Wasko, C., A. Sharma, and S. Westra, 2016b: Reduced spatial extent of extreme storms at higher temperatures. *Geophysical Research Letters*, **43,** 4026-4032.

Weyhenmeyer, G. A., E. Willen, and L. Sonesten, 2004: Effects of an extreme precipitation event on water chemistry and phytoplankton in the Swedish Lake Malaren. *Boreal Environ Res*, **9,** 409-420.

Xiao, C., P. Wu, L. Zhang, and L. Song, 2016: Robust increase in extreme summer rainfall intensity during the past four decades observed in China. *Sci Rep*, **6,** 38506.

Zhao, P., and Coauthors, 2018: The Third Atmospheric Scientific Experiment for Understanding the Earth–Atmosphere Coupled System over the Tibetan Plateau and Its Effects. *Bulletin of the American Meteorological Society*, **99,** 757-776.

List of Figure Caption

Figure 1. Location of the study area (Ganzhou) and selected rainfall stations.

Figure 2. The statistics of the selected rain events. (a) the number of events recorded at each station; (b) the distribution of number of events in terms of station number; (c) the distribution of duration of events in terms of event number; (d) the distribution of total amount of rain in terms of event number.

Figure 3. The procedure on the calculation of temporal concentration index (TCI). (a) calculation of accumulative rain sequence with assumed temporal center marked 1 for the temporal distribution of an actual rain event shown in (b); (c) a hypothetical rain event with uniform distribution of the same total rainfall amount; (d) the cumulative rain curves of the actual rain event and of the hypothetical uniformly distributed rain event; (e) TCIs derived using each point as the temporal center, where the largest value is identified in red as the final TCI.

Figure 4. The procedure on the calculation of spatial concentration index (SCI). (a) An example of a central station and nearby stations within a specified radius; (b) rain at individual stations organized according to their distances from the central station; (c) the accumulative rain amount within a given distance from the central station for an actual rain event (red) and for a hypothetical spatially uniform rain event (blue).

Figure 5. Sample distribution and fitted Beta distribution of TCI for (a) all rain events and (b) events at temperatures below 20 ℃ (blue) and above 20 ℃ (red) where dash lines represent the fitted Beta distributions; (c) cumulative distribution of TCI and (d)

the total number of rain events at temperatures below 20 °C (blue) and above 20 °C (red).

Figure 6. The relationship between bin-average TCI and temperature for (a) all events and the events with rainfall amount beyond the percentile of 50th, 75th, and 90th, respectively, where the bar shows the number of events within each bin; (b) all events with the 95% confidence interval; (c) events with durations of 1-2 hours, 2-3 hours, 3-4 hours, and longer than 4 hours, respectively, where the bars show the number of events within each bin.

Figure 7. The TCI-temperature relationship sensitivity to different duration thresholds (25, 50, and 75 minutes) used for rain event separation, for comparison with Figures 5 and 6. The values of duration threshold are shown at the top of each column.

Figure 8. The distribution of SCI for (a) all rain events, and for (b) events at temperatures below 20 °C (blue) and above 20 °C (red), where the dash lines represent the fitted Wald distributions; (c) cumulative distribution of SCI for events at temperatures below 20°C (blue) and above 20°C (red), and (d) the number of events in different temperature groups.

Figure 9. The relationship between the bin-average SCI and temperature for (a) all events and the events with precipitation amount beyond the 50^{th}, 75^{th}, and 90^{th} percentiles respectively, where the bars show the number of events within each bin; (b) all events with the 95% confidence interval; (c) the relationship between the bin-average SCI and the corresponding duration. Note that SCI is binned according to duration in (c).

Figure 10. The SCI-temperature relationship sensitivity to different radiuses (15, 20, 25, 30, and 40 km), for comparison with Figures 8 and 9. The radius values are shown at the top of each column.

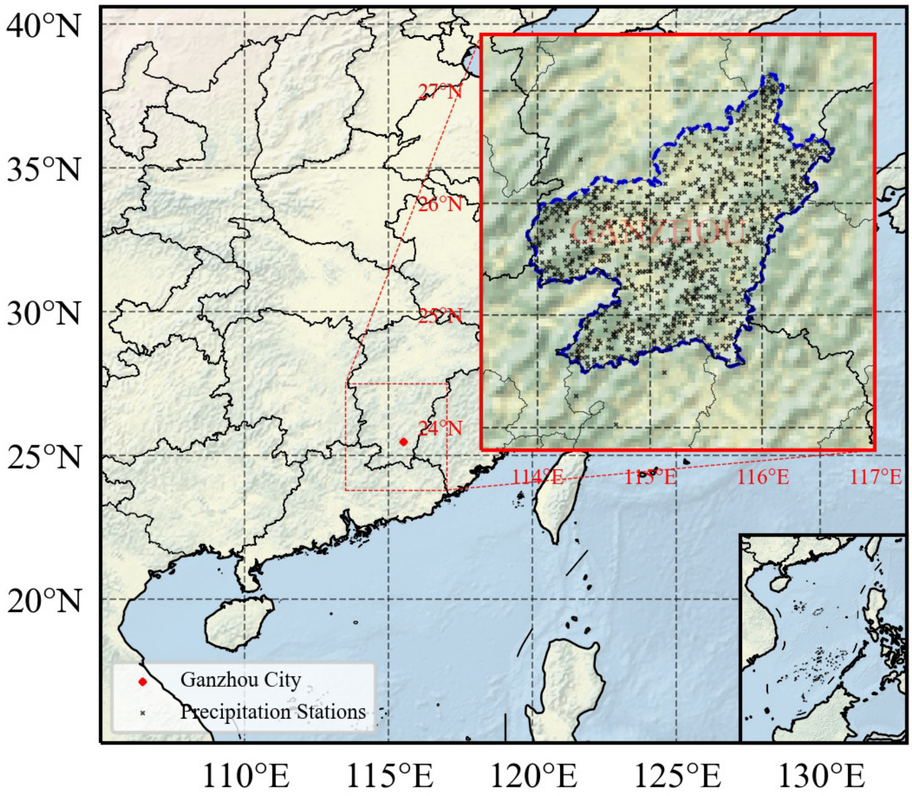

Figure 1. Location of the study area (Ganzhou) and selected rainfall stations.

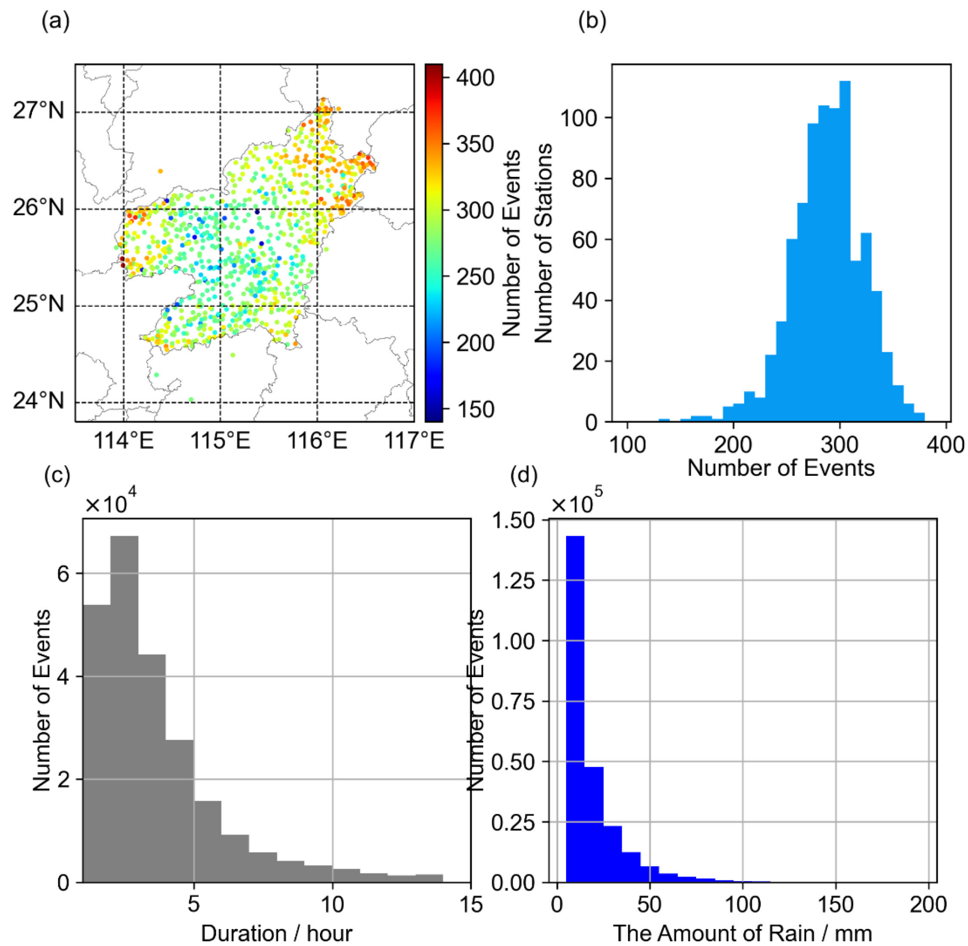

Figure 2. The statistics of the selected rain events. (a) the number of events recorded at each station; (b) the distribution of number of events in terms of station number; (c) the distribution of duration of events in terms of event number; (d) the distribution of total amount of rain in terms of event number.

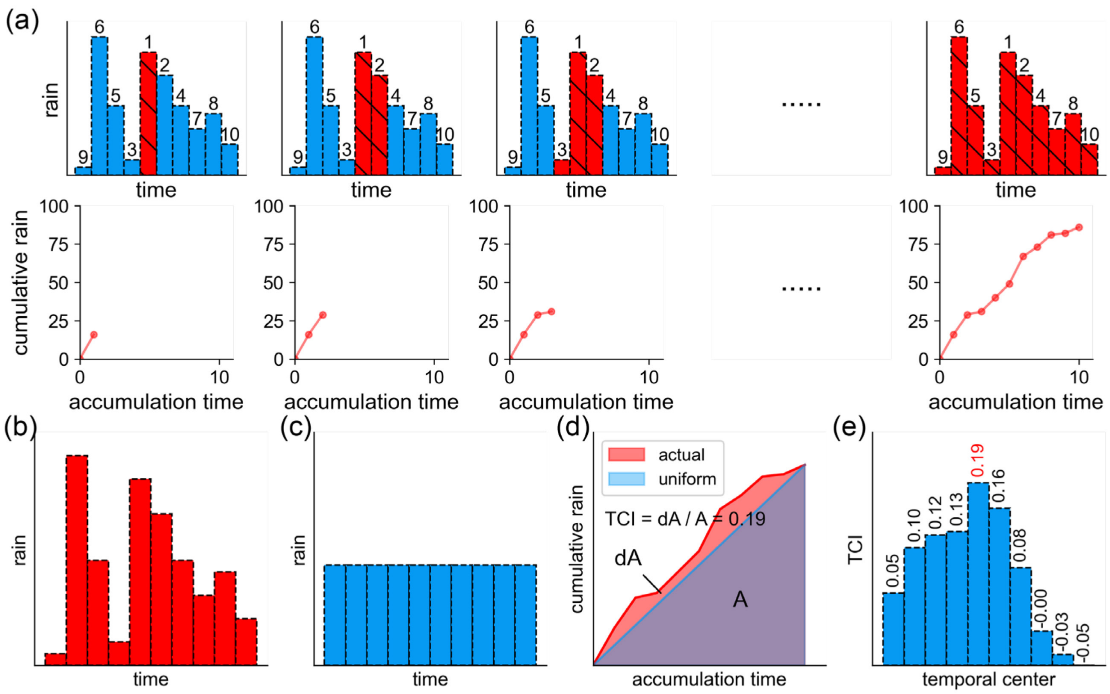

Figure 3. The procedure on the calculation of temporal concentration index (TCI). (a) calculation of accumulative rain sequence with assumed temporal center marked 1 for the temporal distribution of an actual rain event shown in (b); (c) a hypothetical rain event with uniform distribution of the same total rainfall amount; (d) the cumulative rain curves of the actual rain event and of the hypothetical uniformly distributed rain event; (e) TCIs derived using each point as the temporal center, where the largest value is identified in red as the final TCI.

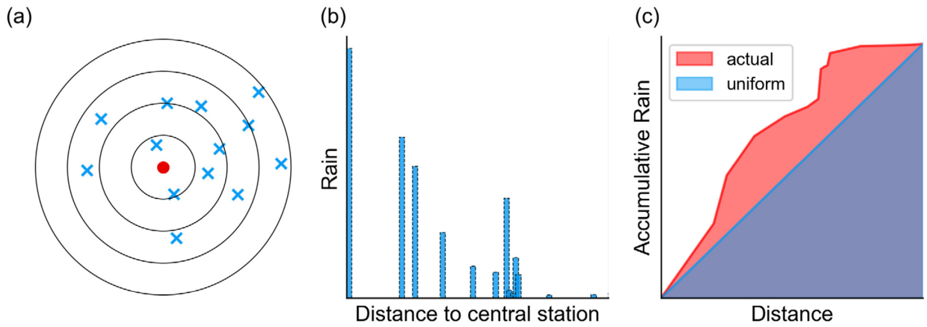

Figure 4. The procedure on the calculation of spatial concentration index (SCI). (a) An example of a central station and nearby stations within a specified radius; (b) rain at individual stations organized according to their distances from the central station; (c) the accumulative rain amount within a given distance from the central station for an actual rain event (red) and for a hypothetical spatially uniform rain event (blue).

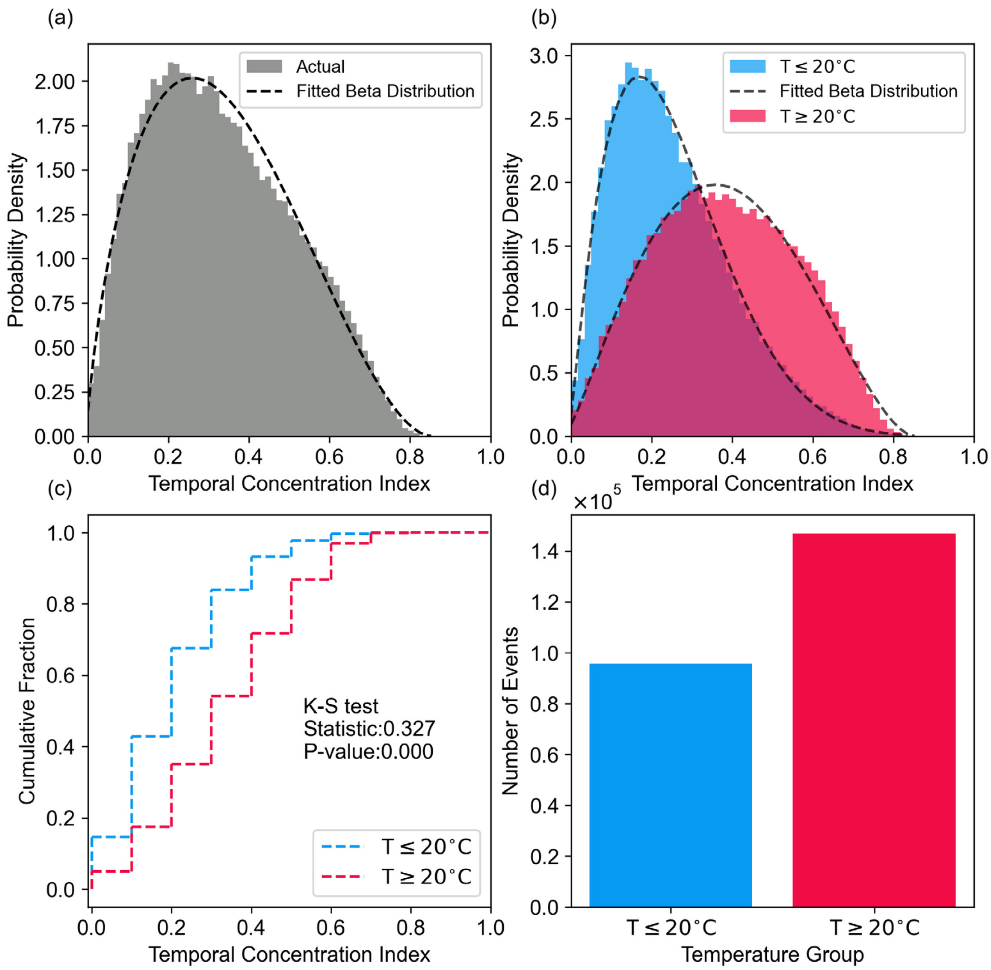

Figure 5. Sample distribution and fitted Beta distribution of TCI for (a) all rain events and (b) events at temperatures below 20 ℃ (blue) and above 20 ℃ (red), where dash lines represent the fitted Beta distributions; (c) cumulative distribution of TCI and (d) the total number of rain events at temperatures below 20 ℃ (blue) and above 20 ℃ (red).

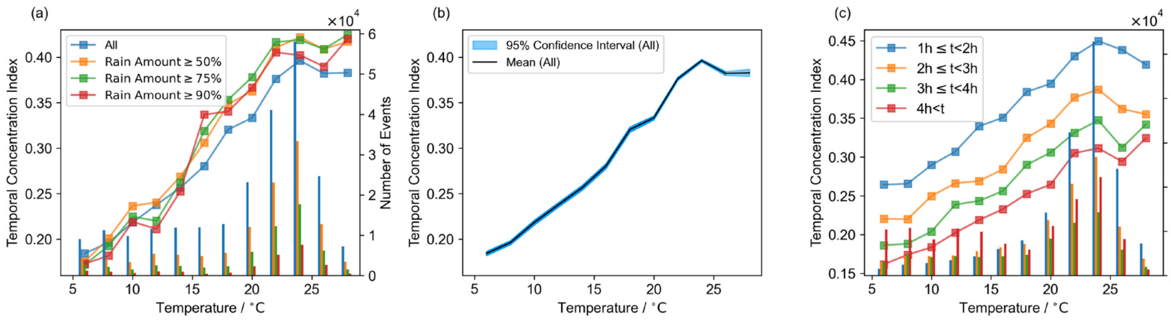

Figure 6. The relationship between bin-average TCI and temperature for (a) all events and the events with rainfall amount beyond the percentile of 50th, 75th, and 90th, respectively, where the bar shows the number of events within each bin; (b) all events with the 95% confidence interval; (c) events with durations of 1-2 hours, 2-3 hours, 3-4 hours, and longer than 4 hours, respectively, where the bars show the number of events within each bin.

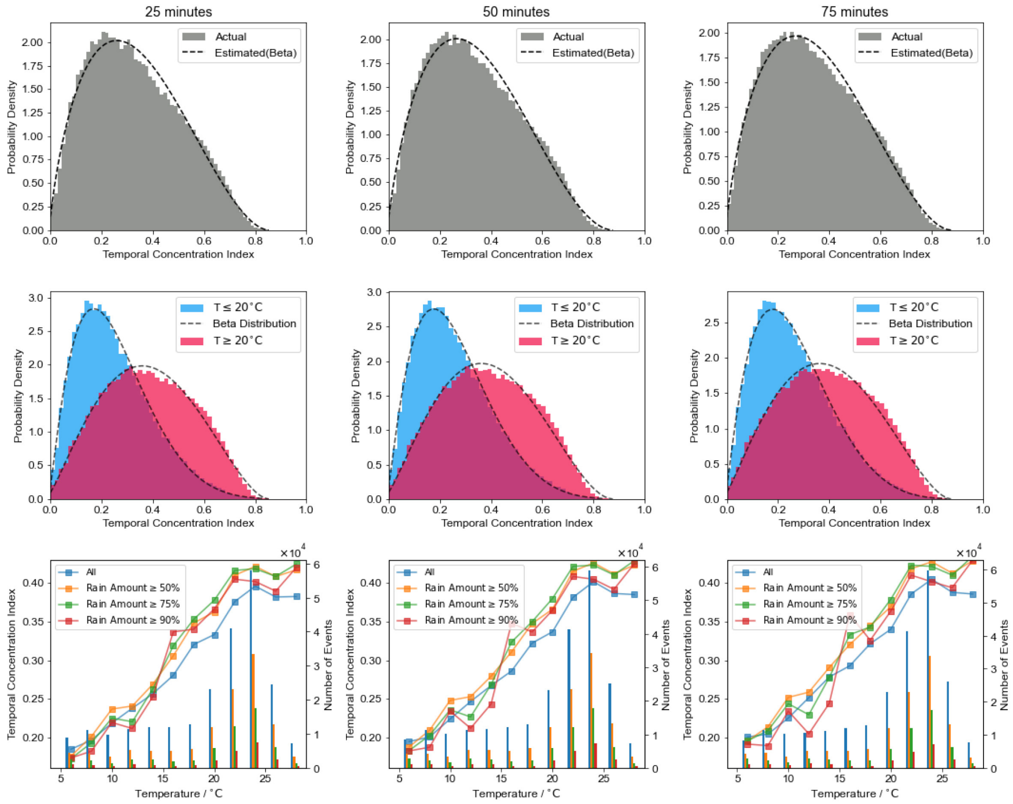

Figure 7. The TCI-temperature relationship sensitivity to different duration thresholds (25, 50, and 75 minutes) used for rain event separation, for comparison with Figures 5 and 6. The values of duration threshold are shown at the top of each column.

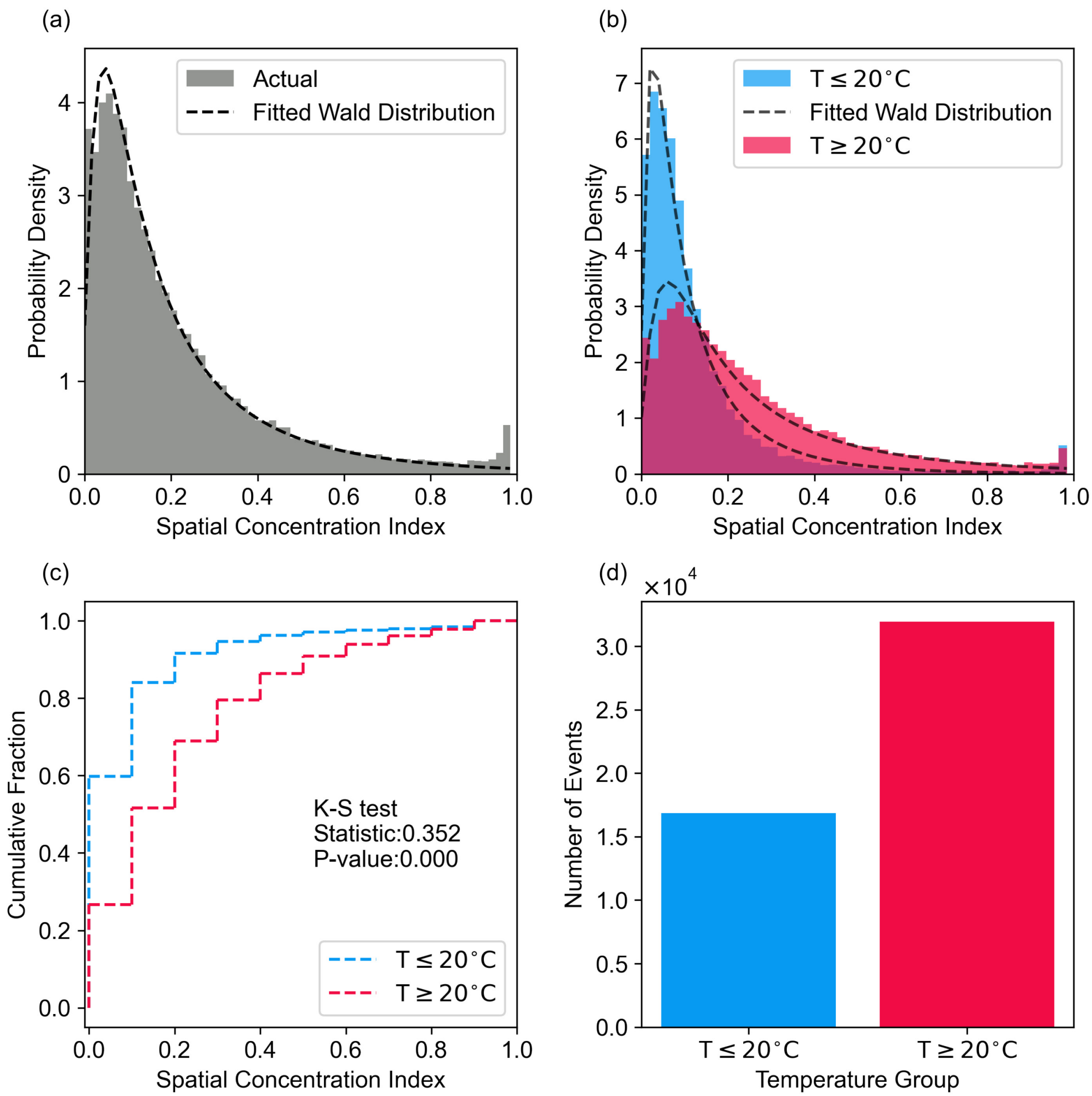

Figure 8. The distribution of SCI for (a) all rain events and for (b) events at temperatures below 20 ℃ (blue) and above 20 ℃ (red), where the dash lines represent the fitted Wald distributions; (c) cumulative distribution of SCI for eventsat temperatures below 20 ℃ (blue) and above 20 ℃ (red), and (d) the number of events in different temperature groups.

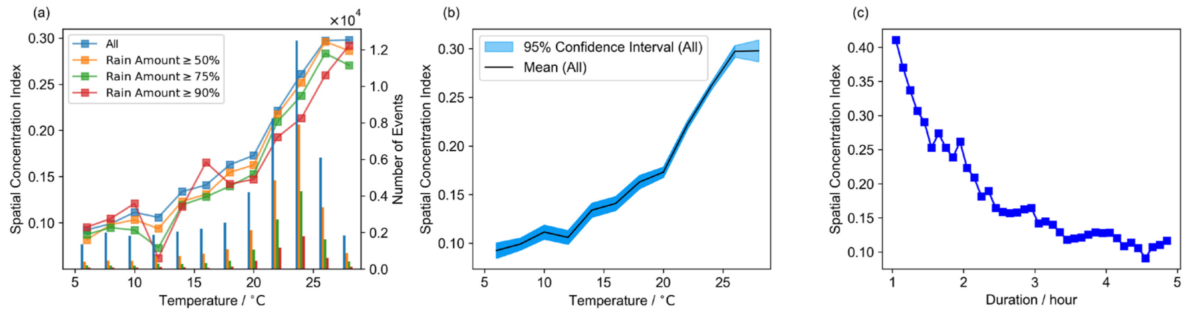

Figure 9. The relationship between the bin-average SCI and temperature for (a) all events and the events with precipitation amount beyond the 50th, 75th, and 90th percentiles respectively, where the bars show the number of events within each bin; (b) all events with the 95% confidence interval; (c) the relationship between the bin-average SCI and the corresponding duration. Note that SCI is binned according to duration in (c).

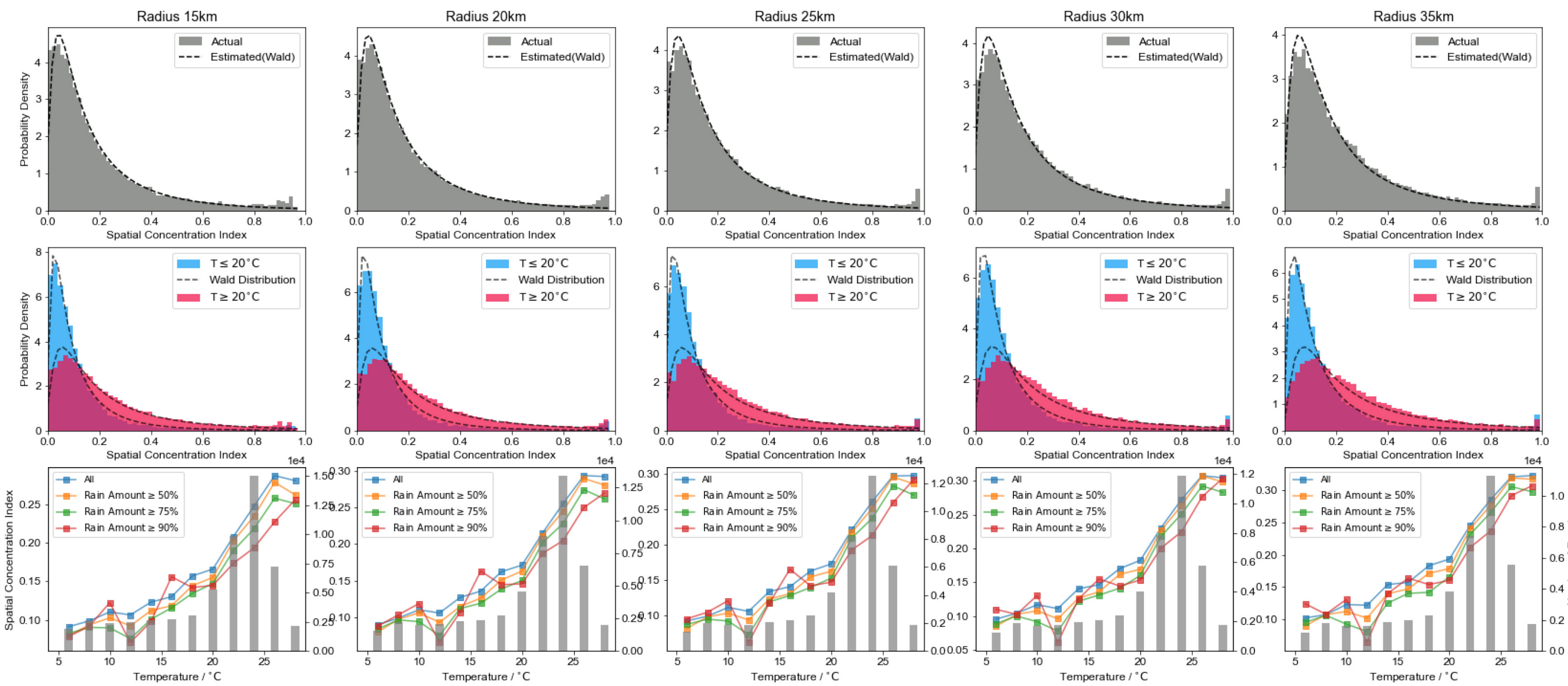

Figure 10. The SCI-temperature relationship sensitivity to different radiuses (15, 20, 25, 30, and 40 km), for comparison with Figures 8 and 9. The radius values are shown at the top of each column.